

# Near-infrared and Millimeter Constraints on the Nuclear Energy Source of the Infrared Luminous Galaxy NGC 4418

Masatoshi Imanishi<sup>1</sup>

*National Astronomical Observatory, 2-21-1, Osawa, Mitaka, Tokyo 181-8588, Japan*

`imanishi@optik.mtk.nao.ac.jp`

Kouichiro Nakanishi, Nario Kuno

*Nobeyama Radio Observatory, Minamimaki, Minamisaku, Nagano, 384-1305, Japan*

`nakanisi@nro.nao.ac.jp, kuno@nro.nao.ac.jp`

and

Kotaro Kohno

*Institute of Astronomy, University of Tokyo, 2-21-1, Osawa, Mitaka, Tokyo, 181-0015, Japan*

`kkohno@ioa.s.u-tokyo.ac.jp`

## ABSTRACT

We present near-infrared and millimeter investigations of the nucleus of the infrared luminous galaxy NGC 4418, which previous observations suggest possesses a powerful buried AGN. We found the following main results: (1) The infrared *K*-band spectrum shows CO absorption features at 2.3–2.4  $\mu\text{m}$  owing to stars and very strong H<sub>2</sub> emission lines. The luminosity ratios of H<sub>2</sub> emission lines are suggestive of a thermal origin, and the equivalent width of the H<sub>2</sub> 1–0 S(1) line is the second largest observed to date in an external galaxy, after the well-studied strong H<sub>2</sub>-emitting galaxy NGC 6240. (2) The infrared *L*-band

---

<sup>1</sup>Visiting Astronomer at the Infrared Telescope Facility, which is operated by the University of Hawaii under Cooperative Agreement no. NCC 5-538 with the National Aeronautics and Space Administration, Office of Space Science, Planetary Astronomy Program.

spectrum shows a clear polycyclic aromatic hydrocarbon (PAH) emission feature at  $3.3 \mu\text{m}$ , which is usually found in star-forming galaxies. The estimated star-formation luminosity from the observed PAH emission can account for only a small fraction of the infrared luminosity. (3) Millimeter interferometric observations of the nucleus reveal a high HCN (1–0) to HCO+ (1–0) luminosity ratio of  $\sim 1.8$ , as has been previously found in pure AGNs. (4) The measurements of HCN (1–0) luminosity using a single-dish millimeter telescope show that the HCN (1–0) to infrared luminosity ratio is slightly larger than the average, but within the scattered range, for other infrared luminous galaxies. All of these results can be explained by the scenario in which, in addition to energetically-insignificant, weakly-obscured star-formation at the surface of the nucleus, a powerful X-ray emitting AGN deeply buried in dust and high density molecular gas is present.

*Subject headings:* galaxies: active — galaxies: nuclei — infrared: galaxies — galaxies: individual (NGC 4418)

## 1. Introduction

Infrared luminous galaxies ( $L_{\text{IR}} \gtrsim 10^{11} L_{\odot}$ ), discovered with the *IRAS* all sky survey, radiate most of their luminosity as dust emission in the infrared (Sanders & Mirabel 1996). Thus, powerful energy sources, either starbursts and/or active galactic nuclei (AGNs), are present hidden behind dust. As the bright end of the local luminosity function is dominated by these infrared luminous galaxies (Soifer et al. 1987), they constitute a very important population in the local universe. At high redshift, these infrared luminous galaxies dominate the cosmic infrared background emission, and have been used to trace the dust-obscured star formation rate, dust content, and metallicity in the early universe, based on the assumption that they are powered by starbursts (Barger, Cowie, & Sanders 1999). Estimating the fraction of their infrared luminosities that is powered by individual activity (i.e., starbursts and AGNs) is fundamental not only to unveil the true nature of these galaxies but also to understand obscured AGN-starburst connections in the universe. As distant sources are too faint to investigate in detail with existing observing facilities, a complete understanding of these infrared luminous galaxies in the nearby universe is a first step to achieving these goals.

If AGNs are present and obscured by dust in a *torus* geometry, then clouds along the torus axis are photo-ionized by the AGN’s hard radiation (these are the so-called narrow line regions: NLRs; Robson 1996). The NLRs produce optical emission lines with flux ratios that are distinguishable from those of normal star-forming galaxies, so AGNs obscured by torus-shaped dust are detectable through optical spectroscopy (classified as Seyferts; Veilleux,

Kim, & Sanders 1999a). Such obscured AGNs are also recognizable by detecting strong high-excitation forbidden emission lines, originating in the NLRs, in high-resolution near- to mid-infrared spectra (Genzel et al. 1998; Veilleux, Sanders, & Kim 1999b). Approximately 10–20% of nearby ( $z < 0.3$ ) infrared luminous galaxies with  $L_{\text{IR}} > 10^{11}L_{\odot}$  are known to possess such AGNs (Veilleux et al. 1999a,b). However, since the nuclear regions of infrared luminous galaxies are very dusty (Sanders & Mirabel 1996), AGNs resident in the majority of these galaxies may be deeply embedded in dust along all sightlines. In such *buried* AGNs, X-ray dissociation regions dominated by low-ionization species (Maloney, Hollenbach, & Tielens 1996) develop, rather than NLRs, so that the signatures of buried AGNs are difficult to find using the conventional methods described above. A recent detailed investigation of the local infrared  $60 \mu\text{m}$  luminosity function has indirectly suggested that buried AGNs may be energetically important in infrared luminous galaxies (Takeuchi et al. 2003). It is desirable to establish a method by which to reveal the presence of buried AGNs more directly and persuasively, and to quantitatively determine their energetic importance in infrared luminous galaxies.

Observations at wavelengths where dust extinction is low are clearly a powerful way to investigate buried AGNs. Some methods have been proposed, including thermal infrared (3–25  $\mu\text{m}$ ) imaging (Soifer et al. 2000) and spectroscopic observations (Genzel et al. 1998; Imanishi & Dudley 2000), millimeter interferometric observations (Kohno et al. 2002), and high energy X-ray observations (Franceschini et al. 2003). Some of these methods have succeeded in providing strong evidence for buried AGNs in some optically-non-Seyfert infrared luminous galaxies. Examples include Arp 299 (Della Ceca et al. 2002), NGC 4945 (Iwasawa et al. 1993; Done, Madejski, & Smith 1996), IRAS 08572+3915 (Dudley & Wynn-Williams 1997; Soifer et al. 2000; Imanishi & Dudley 2000), and UGC 5101 (Imanishi, Dudley, & Maloney 2001; Imanishi & Maloney 2003; Imanishi et al. 2003). However, even in these galaxies, the properties of the energy sources investigated using independent methods are not completely quantitatively consistent, primarily because these sources may be AGN/starburst composites, rather than pure buried AGNs or pure starbursts, and because correction for dust extinction can cause some ambiguity. It is important to observe selected buried AGN candidates in more detail, by combining these potentially powerful methods, and to draw a quantitatively consistent picture of their energy sources.

NGC 4418, at  $z = 0.007$ , is one of the closest and strongest buried AGN candidates. It has an infrared luminosity of  $L_{\text{IR}} \sim 9 \times 10^{10}L_{\odot}$  ( $= 10^{44.5}$  ergs  $\text{s}^{-1}$ ; see Table 1), and shows no clear Seyfert signatures in its optical spectrum (Armus, Heckman, & Miley 1989; Lehnert & Heckman 1995). The 5–23  $\mu\text{m}$  mid-infrared spectrum of NGC 4418 has the typical shape of an obscured AGN (Roche et al. 1991; Spoon et al. 2001). Based on an 8–23  $\mu\text{m}$  mid-infrared spectrum, Dudley & Wynn-Williams (1997) argued that the energy source of NGC

4418 is very compact and more centrally-concentrated than surrounding dust, as is expected for a buried AGN. The core of NGC 4418 is spatially very compact ( $\lesssim 0''.5$ ) in the infrared and radio (Evans et al. 2003; Condon et al. 1990; Eales et al. 1990; Kewley et al. 2000), again suggesting the presence of a compact energy source like an AGN. From far-infrared spectroscopy, NGC 4418 is known to be an unusually weak [CII] ( $158 \mu\text{m}$ ) emitter relative to its far-infrared luminosity (Malhotra et al. 1997, 2000). The presence of a powerful buried AGN is one explanation for this (Malhotra et al. 1997), although some alternative scenarios exist (Malhotra et al. 2001). In this way, evidence for a powerful buried AGN at the center of NGC 4418 has been accumulated. However, the evidence still may not be conclusive (Evans et al. 2003). Further constraints on the nuclear energy source of NGC 4418 from the use of other techniques are clearly warranted. In this paper, we report on near-infrared  $K$ - ( $2.0$ – $2.5 \mu\text{m}$ ) and  $L$ -band ( $2.8$ – $4.1 \mu\text{m}$ ) spectroscopic observations as well as millimeter ( $3.4 \text{ mm}$ ) observations using both a single dish telescope and an interferometric array. Throughout this paper,  $H_0 = 75 \text{ km s}^{-1} \text{ Mpc}^{-1}$ ,  $\Omega_M = 0.3$ , and  $\Omega_\Lambda = 0.7$  are adopted, so that the distance to NGC 4418 is  $28.2 \text{ Mpc}$  and  $1 \text{ arcsec}$  corresponds to  $130 \text{ pc}$ .

## 2. Observations and Data Reduction

### 2.1. Near-infrared spectroscopy

#### 2.1.1. Spectroscopy with SpeX at the IRTF 3-m telescope

Near-infrared spectroscopic observations were performed with SpeX (Rayner et al. 2003) at the IRTF 3-m telescope on Mauna Kea, Hawaii, on 2003 March 18 (UT). The  $1.9$ – $4.2 \mu\text{m}$  cross-dispersed mode with a  $0''.8$  wide slit was employed, so that both  $K$ - ( $2.0$ – $2.5 \mu\text{m}$ ) and  $L$ -band ( $2.8$ – $4.1 \mu\text{m}$ ) spectra were taken simultaneously with a resolution of  $R \sim 1000$ . The sky conditions were photometric and the seeing size at  $K$  was measured to be  $\sim 0''.6$  (full-width at half-maximum; FWHM). The position angle of the slit was set along the north-south direction. A standard telescope nodding technique (ABBA pattern) was employed along the slit to subtract background emission. We set the throw between the A and B positions to be  $7.5 \text{ arcsec}$ , because infrared  $2$ – $20 \mu\text{m}$  emission from NGC 4418 is dominated by the compact nucleus (Scoville et al. 2000; Evans et al. 2003). With this throw, the signal from the object was always inside the slit ( $15 \text{ arcsec}$  long).

The telescope tracking was monitored with the infrared slit-viewer of SpeX. Each exposure was  $15 \text{ sec}$ , and 2 coadds were employed at each position. With this exposure time, signals at  $\lambda_{\text{obs}} > 4.1 \mu\text{m}$  (in the observed frame) exceed the linearity level of the SpeX array, and so data at  $\lambda_{\text{obs}} > 4.1 \mu\text{m}$  were removed. One ABBA cycle results in a 2-min ( $15 \text{ sec} \times$

2 coadds  $\times$  4 positions) exposure time. This cycle was repeated 40 times and so the total net on-source integration time was 80 min.

An F8-type main sequence star, HR 4708, was observed as a standard star, with an airmass difference of  $<0.05$  to NGC 4418, to correct for the transmission of the Earth’s atmosphere. The  $K$ - and  $L$ -band magnitudes of HR 4708 were estimated to be  $K = 5.04$  and  $L = 4.99$  mag, respectively, from its  $V$ -band ( $0.6 \mu\text{m}$ ) magnitude (6.40 mag), adopting the  $V - K$  and  $V - L$  colors of an F8 type main sequence star (Tokunaga 2000).

Standard data reduction procedures were employed using IRAF<sup>1</sup>. First, bad pixels and pixels hit by cosmic rays were replaced with the interpolated values of the surrounding pixels. Then, frames taken with an A (or B) beam were subtracted from frames subsequently taken with a B (or A) beam, and the resulting subtracted frames were added and then divided by a spectroscopic flat image. The spectra of NGC 4418 and HR 4708 were then extracted by integrating signals over  $2''/4$  along the slit. Wavelength calibration was performed using the wavelength-dependent transmission of the Earth’s atmosphere. The NGC 4418 spectrum was divided by that of HR 4708, and was multiplied by the spectrum of a blackbody with  $T_{\text{eff}} = 6000$  K, corresponding to an F8-type main sequence star (Tokunaga 2000). Flux-calibration was made based on the signals detected inside our slit and on the adopted magnitudes of HR 4708.

In the  $L$ -band spectrum, S/N ratios in the continuum are much worse than those in the  $K$ -band, because of the higher background signals from the Earth’s atmosphere in the former. Thus, appropriate spectral binning to  $R \sim 150$  was applied. For an obscured AGN candidate such as NGC 4418, the targeted features in the  $L$ -band are the  $3.1 \mu\text{m}$  absorption feature caused by ice-covered dust grains, the  $3.3 \mu\text{m}$  polycyclic aromatic hydrocarbon (PAH) emission feature, and the  $3.4 \mu\text{m}$  absorption feature due to bare carbonaceous dust grains (Imanishi & Maloney 2003). Since all of these features are spectrally broad, the adopted spectral resolution is sufficient to investigate their properties.

### 2.1.2. Spectroscopy with NIRC at the Keck I 10-m telescope

Since NGC 4418 is a nearby source, the PAH emission, one of the important features used in our scientific interpretation, has a peak at  $3.313 \mu\text{m}$  ( $= 3.29 \mu\text{m} \times 1.007$ ). At 3.31–

---

<sup>1</sup>IRAF is distributed by the National Optical Astronomy Observatories, which are operated by the Association of Universities for Research in Astronomy, Inc. (AURA), under cooperative agreement with the National Science Foundation.

3.32  $\mu\text{m}$  a deep methane absorption feature is present owing to the Earth’s atmosphere, peaking at 3.315  $\mu\text{m}$ , so the transmission of signals from celestial objects is extremely low and the background level is very high, both of which make a spectrum very noisy around this wavelength range. Thus, the determined PAH emission flux can be uncertain if based only on a single spectrum. An independent spectrum taken at a different time with a different instrument is important for a quantitative discussion.

An *L*-band spectrum of NGC 4418 was also taken with NIRC (Matthews & Soifer 1994) at the Keck I 10-m telescope on 2000 March 24 (UT), under clear weather conditions. The LM + gr60 grism was used with a 4.5-pix slit (0.68 wide). The resulting spectral resolution is  $R \sim 70$ . The position angle of the slit was set to  $35^\circ$  east of north. Signals were taken at five positions separated by 4.8 along the slit. Each exposure was 0.41 sec, and 100 coadds were employed at each position. The total net on-source integration time was 41 min (0.41 sec  $\times$  100 coadds  $\times$  5 positions  $\times$  12 cycles). HD 106965 ( $L = 7.295$ ) was observed as a standard star, with an airmass difference of  $<0.05$  to NGC 4418, to correct for the transmission of the Earth’s atmosphere.

Data reduction procedures were carried out using IRAF, in a similar way as those employed for the IRTF SpeX spectrum. First, bias and dark frames were subtracted from each frame, and then the successive frame was subtracted. After flat-field and bad-pixel corrections had been applied, the frames were shifted, and then summed to extract a spectrum. Wavelength calibration was carried out using the wavelength-dependent transmission of the Earth’s atmosphere. The NGC 4418 spectrum was divided by that of HD 106965, multiplied by the spectrum of a blackbody with  $T_{\text{eff}} = 8500$  K, flux-calibrated, and then a final spectrum was obtained.

## 2.2. Millimeter observations

### 2.2.1. Nobeyama 45-m telescope

We used the 45-m telescope of the Nobeyama Radio Observatory (NRO) to measure the luminosity of HCN (1–0) ( $\lambda_{\text{rest}} = 3.3848$  mm or  $\nu_{\text{rest}} = 88.632$  GHz). The half-power beam width (HPBW) of the telescope was  $\sim 19$  arcsec, and the main beam efficiency was  $\sim 0.51$  at this wavelength (frequency). The HCN observations were made on 2002 November 28 (UT), under clear weather conditions. The HCN-line data were taken simultaneously with two SIS receivers, S80 and S100, which can observe two orthogonal polarizations simultaneously. However, the performance of S80 was unstable during our observations, and thus we used only S100 data for our analysis. The receiver backends were 2048 channel wide-band acousto-

optical spectrometers (AOSs). The frequency resolution and the total band width were 250 kHz and 250 MHz, respectively, which correspond to  $0.85 \text{ km s}^{-1}$  and  $850 \text{ km s}^{-1}$  at the observed wavelength (frequency). An intensity calibration was performed using the chopper wheel method. The system noise temperatures (SSB), including the antenna ohmic loss and the Earth’s atmospheric effect, were 230–280 K at the observed wavelength (frequency). The telescope pointing was checked every 50 minutes by observing the bright quasar 3C 273. We used a position-switching mode with an integration time of 20 sec for on- and off-source.

The pointing of the NRO 45-m telescope is very sensitive to wind. To obtain a reliable flux estimate, we used only data taken during calm wind conditions (wind speed  $\lesssim 10 \text{ m s}^{-1}$ ) for the analysis. The total net on-source exposure time for the HCN observations was 5600 sec.

Data analysis was made using the software Newstar and AIPS in a standard manner. In each frame, the stability of the baseline was checked by eye, and data with unstable baselines were removed. The baseline was fit with a first order polynomial function and subtracted from the actual spectrum to show the HCN line spectrum.

### 2.2.2. *RAINBOW Interferometer and Nobeyama Millimeter Array*

Interferometric observations of HCN (1–0) and HCO+ (1–0) ( $\lambda_{\text{rest}} = 3.3637 \text{ mm}$  or  $\nu_{\text{rest}} = 89.188 \text{ GHz}$ ) were performed with the RAINBOW Interferometer at NRO on 2004 January 27 and 28 (UT) under clear and virtually windless (wind speed  $< 5 \text{ m s}^{-1}$ ) observing conditions. The RAINBOW Interferometer is the seven-element combined array that includes six 10-m antennas (Nobeyama Millimeter Array; NMA) and the NRO 45-m telescope. During the daytime of the first observation (January 27), there was snow fall, and frozen ice on the surface of the primary mirror of the 45-m telescope had not melted completely by the time of our night observations. Thus, only six 10-m antennas (i.e., the NMA), with the AB array configuration, were used for the observations. In this AB configuration, the longest baseline was 350 m. On the second night, all seven antennas (i.e., RAINBOW) were used, with a longest baseline of 410 m.

The backend was the Ultra-Wide-Band Correlator, UWBC (Okumura et al. 2000), which was configured to cover 1024 MHz with 128 channels at 8 MHz resolution. The central frequency was set to be 88.29 GHz, so that both the HCN and HCO+ lines redshifted to 88.016 GHz and 88.569 GHz, respectively, were simultaneously observable. The band width of 1024 MHz corresponds to  $\sim 3500 \text{ km s}^{-1}$  at  $\nu \sim 88 \text{ GHz}$ . Since the Hanning window function was applied to reduce side lobes in spectra, the actual resolution was widened to

16 MHz or  $55 \text{ km s}^{-1}$  at  $\nu \sim 88 \text{ GHz}$ . The bright quasar 3C 273 was used to calibrate temporal variations in the visibility amplitude and phase, as well as passband across the 128 channels. As the NRO 45-m telescope is very sensitive to wind, the maser source R-Com was prepared to use as a pointing check. However, wind was very weak on the second night and the visibility amplitudes between the 10-m antennas and the 45-m antenna were sufficiently large throughout the observations. No pointing check was made for the 45-m telescope.

Standard data reduction was employed using the package UVPROC-II developed at NRO (Tsutsumi, Morita, & Umeyama 1997). For the second night’s data, the position dependence of the secondary mirror of the 45-m telescope on elevation was first corrected. For both days’ data, antenna baselines, bandpass properties, and the time variation of visibility amplitude and phase were corrected for, using the 3C 273 data. Data taken during some fraction of the observing time showed large phase scatters, owing to bad radio seeing. As these datasets are useless, they were removed. After clipping a small fraction of unusually high amplitude data, the data were Fourier-transformed using a natural  $uv$  weighting. The flux-calibration of NGC 4418 was made by observing the quasar 1741–038, whose flux level relative to Uranus had been measured. Since the declination of NGC 4418 is almost  $0^\circ$ , strong side lobes were evident along the north-south direction. A conventional CLEAN method was applied to deconvolve the synthesized beam pattern.

### 3. Results

#### 3.1. Near-infrared Spectra

##### 3.1.1. *K*-band

Figure 1 shows a flux-calibrated infrared *K*-band slit spectrum of NGC 4418, taken with IRTF SpeX. The signals integrated over  $0''.8 \times 2''.4$  give  $K = 12.6 \text{ mag}$ , which is in reasonable agreement with previously obtained photometric measurements using small apertures;  $K = 12.8 \text{ mag}$  ( $1''.7$ ) by Eales et al. (1990), or  $K = 13.3 \text{ mag}$  ( $1''.1$ ) and  $K = 11.8 \text{ mag}$  ( $5''$ ) (*HST* NICMOS measurements) by Evans et al. (2003). Thus, slit loss in our spectrum is expected to be insignificant.

Regarding the *K*-band spectrum of NGC 4418, only a low-resolution ( $R \sim 100$ ) spectrum has previously been reported by Ridgway et al. (1994), who argued that the *K*-band spectrum is typical of a normal star-forming galaxy, with the exception of a strong  $\text{H}_2$  1–0 S(1) emission line at  $\lambda_{\text{rest}} = 2.122 \mu\text{m}$ . Our higher resolution ( $R \sim 1000$ ) spectrum newly reveals multiple  $\text{H}_2$  emission lines, and enables quantitative measurements. Important emission lines are



indicated in Figure 1, and their properties are summarized in Table 2. The rest-frame equivalent width of the H<sub>2</sub> 1–0 S(1) emission was measured to be EW<sub>S(1)</sub> = 36 Å, which is significantly larger than in the majority of infrared luminous galaxies ( $\lesssim 20$  Å; Goldader et al. 1997b), and the second highest among galaxies so far known, next to NGC 6240 (=69 Å; Goldader et al. 1997b), the well-studied, unusually strong H<sub>2</sub>-emitting galaxy (Rieke et al. 1985). The H<sub>2</sub> 1–0 S(1) to infrared luminosity ratio is L<sub>S(1)</sub>/L<sub>IR</sub>  $\sim 10^{-5.4}$ . Despite the large equivalent width (EW<sub>S(1)</sub>), the L<sub>S(1)</sub>/L<sub>IR</sub> ratio is in the lowest scattered range observed in infrared luminous galaxies (=10<sup>-5.11±0.28</sup>; Goldader et al. 1997a).

There is a gap in the continuum level of the spectrum between  $\lambda < 2.3 \mu\text{m}$  and  $> 2.3 \mu\text{m}$ . We attribute the gap to CO absorption features at  $\lambda_{\text{rest}} = 2.31\text{--}2.4 \mu\text{m}$ , which are usually found in star-forming galaxies (Goldader et al. 1997b). To estimate the absorption strength, we basically follow the method proposed by Doyon, Joseph, & Wright (1994), who defined a spectroscopic CO index as

$$\text{CO}_{\text{spec}} \equiv -2.5 \log \langle R_{2.36} \rangle, \quad (1)$$

where  $\langle R_{2.36} \rangle$  is the average of actual signals at  $\lambda_{\text{rest}} = 2.31\text{--}2.40 \mu\text{m}$  divided by a power-law continuum ( $F_{\lambda} = \alpha \times \lambda^{\beta}$ ) extrapolated from shorter wavelengths. A continuum level is determined using data points at  $\lambda_{\text{rest}} = 2.0\text{--}2.29 \mu\text{m}$ , excluding obvious emission lines. When CO absorption is present,  $\langle R_{2.36} \rangle$  should be less than unity and thus CO<sub>spec</sub> should have a positive value. The adopted continuum level is shown as a solid line in Figure 1, and we obtain CO<sub>spec</sub> = 0.29. This value is as large as those of many star-forming galaxies (Coziol, Doyon, & Demers 2001) and slightly larger than the previous estimate for this galaxy based on a lower resolution ( $R \sim 100$ ) spectrum (=0.23±0.03; Ridgway et al. 1994).

### 3.1.2. *L*-band

Figures 2a and 2b show flux-calibrated *L*-band spectra taken with IRTF SpeX and Keck NIRC, respectively. The 3.3  $\mu\text{m}$  PAH emission feature is found in both spectra. Its line width appears to be larger in the NIRC spectrum owing to its lower spectral resolution. The SpeX and NIRC spectra give  $L = 12.1$  mag ( $0''.8 \times 2''.4$ ) and  $L=12.3$  ( $0''.7 \times 4''$ ), respectively.

From our slit spectrum taken with SpeX, we find the nuclear  $K - L$  color to be 0.5 mag. In the case of SpeX data, both  $K$ - and  $L$ - band spectra were taken simultaneously under the same observing conditions, toward the same regions of the galaxy, with a similar level of possible slit loss, so that the measured  $K - L$  color of 0.5 mag can be taken to be more certain than the absolute  $K$ - and  $L$ -band magnitudes. The nuclear  $K - L$  color is typical of star-forming galaxies (Willner et al. 1984).

The flux of the 3.3  $\mu\text{m}$  PAH emission was estimated using the spectral profile of type-1 sources (Tokunaga et al. 1991) as a template for the 3.3  $\mu\text{m}$  PAH emission, as was made by Imanishi (2002, 2003). The SpeX and NIRC spectra give a 3.3  $\mu\text{m}$  PAH emission flux of  $f_{3.3\text{PAH}} \sim 6$  and  $8 \times 10^{-14}$  ergs  $\text{s}^{-1} \text{cm}^{-2}$ , respectively. We adopt  $f_{3.3\text{PAH}} = 7 \times 10^{-14}$  ergs  $\text{s}^{-1} \text{cm}^{-2}$ , in which case the luminosity and rest-frame equivalent width of the 3.3  $\mu\text{m}$  PAH emission are  $L_{3.3\text{PAH}} \sim 7 \times 10^{39}$  ergs  $\text{s}^{-1}$  and  $\text{EW}_{3.3\text{PAH}} \sim 70$  nm, respectively. The spectral shape of NGC 4418, with a large  $\text{EW}_{3.3\text{PAH}}$  ( $\sim 70$  nm), is also typical of star-forming galaxies (Imanishi & Dudley 2000).

## 3.2. Millimeter Data

### 3.2.1. Single dish data

Figure 3 shows a spectrum of the HCN (1–0) line taken with the NRO 45-m telescope. Using a Gaussian fit, we estimate the HCN flux to be 3.5 K  $\text{km s}^{-1}$ . The HCN flux, estimated based on a simple summation of signals above an adopted continuum level, gives a value consistent within 15%. By adopting the Jy-to-K conversion factor of the NRO 45-m telescope ( $\sim 2.4$  Jy  $\text{K}^{-1}$ ), we obtain an HCN flux of 8.5 Jy  $\text{km s}^{-1}$ . Using equation (1) of Gao & Solomon (2004a), we estimate the HCN luminosity to be  $2.6 \times 10^7$  K  $\text{km s}^{-1} \text{pc}^2$ . Figure 4 compares the infrared to HCN luminosity ratio of NGC 4418 with those of other infrared luminous galaxies. The ratio for NGC 4418 is slightly higher than the average, but within the scattered range, of the ratios found in infrared luminous galaxies.

### 3.2.2. Interferometric data

A nuclear spectrum before continuum subtraction taken with the interferometric array showed that the flux level in between the HCN (1–0) and HCO+ (1–0) emission lines is significantly above the zero level, suggesting that continuum emission is detected. We combined data points that were unaffected by the HCN and HCO+ emission lines and estimated the continuum flux to be  $\sim 8.5$  mJy at  $\lambda \sim 3.4$  mm ( $\nu \sim 88$  GHz). Figure 5 displays the contours of the continuum emission. The continuum emission is spatially compact, and the peak position is spatially coincident with the optical nucleus (J1950;  $12^{\text{h}}26^{\text{m}}54.62^{\text{s}}$ ,  $-00^{\circ}52'39''.20$ ).

After the estimated continuum had been subtracted, we investigated the HCN and HCO+ emission lines from NGC 4418. Figure 6 shows the channel map around the HCN and HCO+ lines. The HCN and HCO+ emission lines are also spatially compact and are spatially coincident with the optical peak.

Figure 7 shows a continuum-subtracted nuclear spectrum around the HCN and HCO+ emission lines. The integrated fluxes of HCN and HCO+ at the peak position are estimated to be  $S_{\text{HCN}} = 10.3 \text{ Jy km s}^{-1}$  and  $S_{\text{HCO}^+} = 5.6 \text{ Jy km s}^{-1}$ , respectively. We thus obtain an HCN-to-HCO+ flux ratio of 1.84 at the NGC 4418 nucleus. Although the *absolute* flux calibration uncertainty of the RAINBOW data can be as large as  $\sim 20\%$ , the HCN-to-HCO+ flux *ratio* should be very reliable, because both lines were observed simultaneously with the same receiver and same correlator unit.

The estimated HCN flux values based on the interferometric array ( $=10.3 \text{ Jy km s}^{-1}$ ) and on the NRO 45-m telescope ( $=8.5 \text{ Jy km s}^{-1}$ ) agree within the absolute flux calibration uncertainty ( $\sim 20\%$ ), suggesting that the bulk of the HCN emission from NGC 4418 is spatially compact and is detected with the interferometric data.

## 4. Discussion

### 4.1. Nuclear star formation

The CO absorption features found in the near-infrared  $K$ -band spectrum originate in stars and not an AGN (Ivanov et al. 2000). The  $3.3 \mu\text{m}$  PAH emission feature also comes from star-forming activity, rather than a pure AGN (Moorwood 1986; Imanishi & Dudley 2000). The nuclear  $K - L$  color of 0.5 mag measured with SpeX data is similar to that of star-forming galaxies (Willner et al. 1984), and much bluer than the typical colors observed in many Seyfert nuclei (Alonso-Herrero et al. 2003; Imanishi & Alonso-Herrero 2004). All of these results suggest that star-forming activity is the dominant contributor to the observed nuclear  $K$ - and  $L$ -band fluxes, as was argued by Spoon et al. (2001) based on the infrared spectral energy distribution of NGC 4418.

The nature of the detected nuclear star formation in NGC 4418 can be investigated using the observed  $3.3 \mu\text{m}$  PAH emission luminosity. In NGC 4418, the  $3.3 \mu\text{m}$  PAH luminosity ( $= 7 \times 10^{39} \text{ ergs s}^{-1}$ ) comes from regions at  $\sim 2 \text{ arcsec}^2$  or  $\sim 0.033 \text{ kpc}^2$ . Thus, its surface brightness is  $S_{3.3\text{PAH}} \sim 2 \times 10^{41} \text{ ergs s}^{-1} \text{ kpc}^{-2}$ . This corresponds to the infrared surface brightness with  $\sim 2 \times 10^{44} \text{ ergs s}^{-1} \text{ kpc}^{-2}$  (Mouri et al. 1990; Imanishi 2002), or the estimated star formation rate per unit area with  $\sim 9 \text{ M}_{\odot} \text{ yr}^{-1} \text{ kpc}^{-2}$  (Kennicutt 1998). This value substantially exceeds the lower limit of  $10^{-1} \text{ M}_{\odot} \text{ yr}^{-1} \text{ kpc}^{-2}$  beyond which superwind activity, a characteristic property of starbursts, can occur (Heckman 2001). We thus conclude that the detected  $3.3 \mu\text{m}$  PAH emission comes from nuclear starbursts, rather than central regions of quiescent star-forming activity in the host galaxy.

The measured  $3.3 \mu\text{m}$  PAH to infrared luminosity ratio in NGC 4418 is  $\sim 2 \times 10^{-5}$ ,

which is a factor of  $\sim 50$  smaller than starburst-dominated galaxies ( $\sim 10^{-3}$ ; Mouri et al. 1990; Imanishi 2002), suggesting that the detected nuclear starbursts, with modest dust extinction in the near-infrared 3–4  $\mu\text{m}$ , contribute very little to the total infrared luminosity of NGC 4418. Since the infrared luminosity is likely to come from the compact nuclear core (Evans et al. 2003), rather than extended star formation in the host galaxy, the dominant energy source, an AGN and/or very compact starbursts, should be deeply buried at the core.

#### 4.2. The Nature of the Buried Energy Source: Signatures of an AGN

Figure 8 shows a plot of the HCN (1–0) to CO (1–0) ( $\lambda_{\text{rest}} = 2.6 \text{ mm}$ ) and HCN (1–0) to HCO+ (1–0) luminosity ratios of NGC 4418 and other nearby galaxies. Empirically, a pure AGN (with no detectable nuclear star-forming activity) shows high HCN/HCO+ and HCN/CO luminosity ratios, as compared to star-forming galaxies (Kohno et al. 2002, 2003). Since HCN traces much higher-density molecular gas ( $n_{\text{H}} \sim 10^4 \text{ cm}^{-3}$ ) than is traced by CO ( $n_{\text{H}} \sim 10^2 \text{ cm}^{-3}$ ), the HCN/CO ratio can vary depending on the density of molecular gas. However, both HCN and HCO+ probe molecular gas of similar density ( $n_{\text{H}} \sim 10^4 \text{ cm}^{-3}$ ), so that the HCN/HCO+ ratio is robust to the density of molecular gas. The high HCN/HCO+ ratio in an AGN may be owing to the enhancement of HCN in molecular gas irradiated by strong X-ray emission from the AGN (Lepp & Dalgarno 1996). Although a full explanation for this high HCN/HCO+ ratio in an AGN is still to be developed, this empirical method can be used to find a buried AGN, because of negligible dust extinction in the millimeter wavelength range. The high HCN/HCO+ luminosity ratio at the nucleus of NGC 4418 suggests the presence of a buried AGN.

The strong CO absorption in the near-infrared  $K$ -band, and strong 3.3  $\mu\text{m}$  PAH emission in the  $L$ -band, suggest that emission from normal star-formation has an important contribution to the observed fluxes in these wavelength ranges. However, the  $\text{H}_2$  emission in the  $K$ -band spectrum is unusually strong as compared to that of normal star-forming galaxies (Ridgway et al. 1994). In normal star-forming galaxies, the  $\text{H}_2$  1–0 S(1) to Br $\gamma$  emission-line luminosity ratios ( $L_{\text{S}(1)}/L_{\text{Br}\gamma}$ ) are smaller than or comparable to unity (Mouri et al. 1989; Mouri & Taniguchi 1992; Goldader et al. 1997b; Coziol, Doyon, & Demers 2001). The  $L_{\text{S}(1)}/L_{\text{Br}\gamma}$  ratio of  $>8$  (Table 2) in NGC 4418 is unusually large. Together with the large  $\text{H}_2$  equivalent width ( $\text{EW}_{\text{S}(1)}$ ) of NGC 4418, this suggests that in addition to emission from normal star-forming activity, some mechanism that can produce strong  $\text{H}_2$  emission should exist at the nucleus of NGC 4418.

Figure 9 shows the luminosity ratios of some  $\text{H}_2$  emission lines. The small observed 2–1 S(1) to 1–0 S(1) luminosity ratio with  $<0.3$  is incompatible with the non-thermal (UV

fluorescence) model as the primary emission mechanism for the detected strong H<sub>2</sub> emission, and favors H<sub>2</sub> emission of thermal origin. Based on the available H<sub>2</sub> data alone, some thermal models, including shocks, X-ray heating, and UV, are not clearly distinguishable. However, the measured HCN/HCO+ ratio can help to distinguish among these scenarios.

In the case of the strong H<sub>2</sub>-emitting galaxy NGC 6240, the H<sub>2</sub> emission was found to be of thermal origin (Sugai et al. 1997), and to come from regions between the double nucleus of NGC 6240 (Sugai et al. 1997). Shocks driven by a galaxy-merger or superwind have been proposed as the primary mechanism of the H<sub>2</sub> emission (Rieke et al. 1985; Van der Werf et al. 1993; Ohyama et al. 2000; Ohyama, Yoshida, & Takata 2003). From these shock regions, a low HCN/HCO+ ratio with  $\sim 0.67$  was observed (Nakanishi et al. 2004). The low HCN/HCO+ ratio in shock regions may be due to the enhancement of HCO+ (Rawlings, Taylor, & Williams 2000; Rawlings et al. 2004). However, NGC 4418 is a single nucleus source, with no clear signs of recent galaxy-merger/interaction (Eales et al. 1990; Evans et al. 2003). Furthermore, at the nucleus of NGC 4418, a high HCN/HCO+ ratio was measured, as found in pure AGNs. Given that stellar UV heating of molecular gas is also expected to show a low HCN/HCO+ ratio (Kohno et al. 2002), X-ray heating of H<sub>2</sub> molecules caused by the putative buried AGN (Draine & Woods 1990) seems plausible. The observed H<sub>2</sub> line luminosity ratios are consistent with this X-ray heating scenario, if the H<sub>2</sub> emission suffers from dust extinction with  $A_K \sim$  several mag (see Fig.9).

NGC 4418 is known to show a very strong 9.7  $\mu\text{m}$  silicate dust absorption feature, whose optical depth was measured to be  $\tau_{9.7} = 5.6\text{--}7$  (Roche et al. 1986; Dudley & Wynn-Williams 1997; Spoon et al. 2001). Adopting the relation of  $\tau_{9.7}/A_V = 0.05\text{--}0.1$  established in the Galactic interstellar medium (Roche & Aitken 1984, 1985), we obtain a dust extinction toward the  $\sim 10 \mu\text{m}$  continuum emitting regions of  $A_V > 50$  mag, or  $A_K > 5$  mag (Rieke & Lebofsky 1985). In the case of a dust envelope around a buried AGN (= a centrally concentrated energy source), dust has a strong temperature gradient in that inner (outer) dust has a higher (lower) temperature. The 10  $\mu\text{m}$  continuum typically comes from 300-K dust, which is located in the outer parts, compared to the innermost dust sublimation radius ( $T = 1000\text{--}1500$  K). Thus, the estimated  $A_V$  traces the dust column toward some outer part of the dust envelope around the buried AGN. H<sub>2</sub> emission excited by X-rays also comes from some outer regions of the dust envelope, similarly to the 300-K dust. If we adopt a value for the dust extinction toward the H<sub>2</sub>-emitting regions of  $A_K > 5$  mag, the model prediction of X-ray heating in Figure 9 will go down, and move slightly to the right, which is consistent with the current observational constraints on the H<sub>2</sub> emission line luminosity ratios.

The scenario of X-ray heating by the buried AGN can also explain the following observational results: (1) the large H<sub>2</sub> S(1) to Br $\gamma$  luminosity ratio, (2) the large equivalent width

of the H<sub>2</sub> 1–0 S(1) emission line ( $EW_{S(1)}$ ), and (3) the small H<sub>2</sub> S(1) to infrared luminosity ratio ( $L_{S(1)}/L_{IR}$ ). On point (1), AGNs generally show significantly larger H<sub>2</sub> 1–0 S(1) to Br $\gamma$  luminosity ratios ( $L_{S(1)}/L_{Br\gamma} > 1$ ) than do star-forming galaxies ( $< 1$ ; Mouri & Taniguchi 1992). On point (2), the H<sub>2</sub> equivalent width ( $EW_{S(1)}$ ) of NGC 4418 is in the highest range observed for AGNs (Mouri & Taniguchi 1992). In a buried AGN, the covering fraction of the central AGN by molecular gas is higher than that of a typical AGN surrounded by torus-shaped molecular gas. This higher covering fraction can produce stronger X-ray heated H<sub>2</sub> emission. Additionally, the near-infrared *K*-band continuum from an AGN originates mostly from 1000- to 1500-K dust close to the innermost, dust sublimation radius (Barvainis 1987). The high obscuration toward the central AGN in NGC 4418, as is implied from the presence of one of the strongest 9.7  $\mu$ m silicate dust absorption features observed (Roche et al. 1991), can significantly attenuate the AGN-originated *K*-band continuum flux. The flux attenuation of H<sub>2</sub> emission from some outer part of the dust envelope is slightly smaller than the *K*-band continuum, producing a higher H<sub>2</sub> equivalent width than in the case of unobscured AGNs. Finally, on point (3), since the H<sub>2</sub> emission from the buried AGN in NGC 4418 is likely to be more highly dust obscured than typical AGNs, the small  $L_{S(1)}/L_{IR}$  ratio can be explained by dust extinction.

With dust extinction of  $A_K > 5$  mag, the dereddened H<sub>2</sub> 1–0 S(1) luminosity becomes  $> 1.3 \times 10^{41}$  ergs s<sup>-1</sup>, and the dereddened  $L_{S(1)}$  to  $L_{IR}$  ratio is  $> 4 \times 10^{-4}$ . The intrinsic X-ray luminosity that produces this H<sub>2</sub> 1–0 S(1) luminosity is estimated to be  $L_X(1-10\text{keV}) > 1 \times 10^{44}$  ergs s<sup>-1</sup> (Lepp & McCray 1983). The resulting 1–10 keV X-ray to infrared luminosity ratio is  $L_X(1-10\text{keV})/L_{IR} > 0.3$ , which is as high as those in AGN-powered infrared luminous galaxies (Risaliti et al. 2000). Thus, in this X-ray heated H<sub>2</sub> emission scenario, the putative buried AGN could account for the bulk of the infrared luminosity from NGC 4418.

In summary, all the data newly available from our observations, including the high HCN/HCO+ ratio, H<sub>2</sub> emission line luminosity ratios, large H<sub>2</sub> to Br $\gamma$  luminosity ratio, and large H<sub>2</sub> equivalent width, can be consistently explained by the buried AGN scenario.

The infrared to HCN luminosity ratio of NGC 4418 is located in the highest part of the scattered range of infrared luminous starburst galaxies (Figure 4). If this ratio is similar to that of starburst galaxies, it is sometimes used to argue that the infrared luminosity of a source is starburst-powered (Gao & Solomon 2004b). However, it simply indicates that much of the infrared emission arises from dust in dense molecular clouds (probed by HCN) whatever the energy source of the luminosities may be (Barvainis et al. 1997; Imanishi & Maloney 2003). The buried AGN in NGC 4418 is most likely to be surrounded by high density gas, as is the case for stars at the star-forming cores of starburst galaxies, and so the similar infrared-to-HCN ratio of NGC 4418 to that of starburst galaxies is quite reasonable.

The presence of buried AGNs in some non-Seyfert ultraluminous infrared galaxies (ULIRGs) with  $L_{\text{IR}} > 10^{12}L_{\odot}$  has been revealed from  $L$ -band spectra, based on significantly lower equivalent widths of the  $3.3 \mu\text{m}$  PAH emission feature ( $\text{EW}_{3.3\text{PAH}}$ ) than starbursts, with strong absorption features (Imanishi & Dudley 2000; Imanishi, Dudley, & Maloney 2001; Imanishi & Maloney 2003), whereas NGC 4418 shows no such signature in the  $L$ -band spectrum. This  $L$ -band spectroscopic method to find a buried AGN is possible only if the AGN-powered dust emission contributes significantly to the observed flux. In ULIRGs, this is often the case (Farrah et al. 2003). However, in the case of NGC 4418, the observed  $L$ -band flux is unfortunately dominated by stellar emission, rather than dust emission (Spoon et al. 2001), making it difficult to find the buried AGN signatures in the  $L$ -band spectrum.

The buried AGN scenario in NGC 4418 presumes the presence of an intrinsically strong X-ray emitting energy source. No significant X-ray emission was detected at  $E < 10 \text{ keV}$  (Maiolino et al. 2003). It has been found that AGNs in roughly half of Seyfert-2 galaxies suffer from Compton-thick ( $N_{\text{H}} > 10^{24} \text{ cm}^{-2}$ ) absorption (Risaliti, Maiolino, & Salvati 1999). In a Compton-thick AGN, the observed 2–10 keV emission is dominated by a scattered/reflected component, rather than a direct, transmitted component, making the observed 2–10 keV flux very weak. The significantly deeper  $9.7 \mu\text{m}$  silicate dust absorption feature in NGC 4418 as compared to typical Seyfert-2 galaxies (Roche et al. 1991) makes it very likely that the putative AGN in NGC 4418 is obscured by Compton-thick absorbing material. Sensitive X-ray observations at  $E > 10 \text{ keV}$  are most desirable to unveil the presence of such a Compton-thick buried AGN, as found in a few non-Seyfert infrared luminous galaxies, NGC 4945 (Iwasawa et al. 1993), Arp 299 (Della Ceca et al. 2002), and NGC 6240 (Vignati et al. 1999).

## 5. Summary

We investigated the nuclear energy source of the infrared luminous galaxy NGC 4418 through near-infrared  $K$ - and  $L$ -band spectroscopy, and millimeter observations at  $\lambda \sim 3.4 \text{ mm}$  using both a single dish telescope and an interferometric array. Various previous observations have suggested that this galaxy has a deeply buried AGN at the center. In the near-infrared spectra, we detected clear PAH emission and CO absorption features, suggesting that the observed near-infrared flux comes mostly from star-forming activity. The magnitude of this detected star-forming activity was measured from the observed PAH emission luminosity and was found to account for only 1/50 of the infrared luminosity of this galaxy. We therefore suggested that the primary energy source of NGC 4418 is deeply buried in dust.

In the near-infrared  $K$ -band spectrum and millimeter interferometric data, large-equivalent-width  $H_2$  emission and a high HCN/HCO+ luminosity ratio, respectively, were found, both of which are naturally explained by the presence of a strong X-ray emitting source, such as an AGN, at the center of NGC 4418. The measured HCN to infrared luminosity ratio in NGC 4418 can also be explained by the AGN scenario, if the AGN is deeply buried in high-density molecular gas and dust. Overall, our new near-infrared and millimeter data supported the buried AGN scenario in NGC 4418.

We are grateful to S. B. Bus, P. Sears (IRTF), R. Campbell, C. Sorenson, W. Wack (Keck), H. Mikoshiba, Y. Iizuka, S. Ishikawa, K. Miyazawa, C. Miyazawa, and A. Sakamoto (NRO) for their support during our observing runs. NRO is a branch of the National Astronomical Observatory, National Institutes of Natural Sciences, Japan. Some parts of the data analysis were made using a computer system operated by the Astronomical Data Analysis Center (ADAC) and the Subaru Telescope of the National Astronomical Observatory. Some of the data presented herein were obtained at the W.M. Keck Observatory, while MI was staying at the Institute for Astronomy, University of Hawaii. MI is grateful to A. T. Tokunaga for giving him the opportunity for the stay, which was financially supported by the Japan Society for the Promotion of Science. The W.M. Keck Observatory is operated as a scientific partnership among the California Institute of Technology, the University of California and the National Aeronautics and Space Administration. The observatory was made possible by the generous financial support of the W.M. Keck Foundation. The authors wish to recognize and acknowledge the very significant cultural role and reverence that the summit of Mauna Kea has always had within the indigenous Hawaiian community. We are most fortunate to have the opportunity to conduct observations from this mountain.



## REFERENCES

- Alonso-Herrero, A., Quillen, A. C., Rieke, G. H., Ivanov, V., & Efstathiou, A. 2003, *AJ*, 126, 81
- Armus, L., Heckman, T. M., & Miley, G. K. 1989, *ApJ*, 347, 727
- Barger, A. J., Cowie, L. L., & Sanders, D. B. 1999, *ApJ*, 518, L5
- Barvainis, R. 1987, *ApJ*, 320, 537
- Barvainis, R., Maloney, P., Antonucci, R., & Alloin, D. 1997, *ApJ*, 484, 695
- Condon, J. J., Helou, G., Sanders, D. B., & Soifer, B. T. 1990, *ApJS*, 73, 359
- Coziol, R., Doyon, R., & Demers, S. 2001, *MNRAS*, 325, 1081
- Della Ceca, R. et al. 2002, *ApJ*, 581, L9
- Done, C., Madejski, G. M., & Smith, D. A. 1996, *ApJ*, 463, L63
- Doyon, R., Joseph, R. D., & Wright, G. S. 1994, *ApJ*, 421, 101
- Draine, B. T., & Woods, D. T. 1990, *ApJ*, 363, 464
- Dudley, C. C., & Wynn-Williams, C. G. 1997, *ApJ*, 488, 720
- Eales, S. A., Becklin, E. E., Hodapp, K. -W., Simons, D. A., & Wynn-Williams, C. G. 1990, *ApJ*, 365, 478
- Evans, A. S. et al. 2003, *AJ*, 125, 2341
- Farrah, D., Afonso, J., Efstathiou, A. Rowan-Robinson, M., Fox, M., & Clements, D. 2003, *MNRAS*, 343, 585
- Franceschini, A. et al. 2003, *MNRAS*, 343, 1181
- Gao, Y., & Solomon, P. M. 2004a, *ApJS*, 152, 63
- Gao, Y., & Solomon, P. M. 2004b, *ApJ*, 606, 271
- Genzel, R. et al. 1998, *ApJ*, 498, 579
- Goldader, J. D., Joseph, R. D., Doyon, R., & Sanders, D. B. 1997a, *ApJ*, 474, 104
- Goldader, J. D., Joseph, R. D., Doyon, R., & Sanders, D. B. 1997b, *ApJS*, 108, 449

- Heckman, T. M. 2001, in ASP Conf. Ser. 240, Gas and Galaxy Evolution, ed. J. E. Hibbard, M. Rupen, & J. H. van Gorkomastro (San Francisco: ASP), 345 (astro-ph/0009075)
- Imanishi, M. 2002, ApJ, 569, 44
- Imanishi, M. 2003, ApJ, 599, 918
- Imanishi, M., & Alonso-Herrero, A. 2004, ApJ, 614, in press (astro-ph/0407215)
- Imanishi, M., & Dudley, C. C. 2000, ApJ, 545, 701
- Imanishi, M., & Maloney, P. R. 2003, ApJ, 588, 165
- Imanishi, M., Dudley, C. C., & Maloney, P. R. 2001, ApJ, 558, L93
- Imanishi, M., Terashima, Y., Anabuki, N., & Nakagawa, T. 2003, ApJ, 596, L167
- Ivanov, V. D., Rieke, G. H., Groppi, C. E., Alonso-Herrero, A., Rieke, M. J., & Engelbracht, C. W. 2000, ApJ, 545, 190
- Iwasawa, K., Koyama, K., Awaki, H., Kunieda, H., Makishima, K., Tsuru, T., Ohashi, T., & Nakai, N. 1993, ApJ, 409, 155
- Kennicutt, R. C. Jr. 1998, ARA&A, 36, 189
- Kewley, L. J., Heisler, C. A., Dopita, M. A., Sutherland, R., Norris, R. P., Reynolds, J. & Lumsden, S. 2000, ApJ, 530, 704
- Kohno, K., Matsushita, S., Vila-Vilaro, B., Okumura, S. K., Shibatsuka, T., Okiura, M., Ishizuki, S., Kawabe, R. 2002, in ASP Conf. Ser. 249, The Central kpc of Starbursts and AGN, ed. J. H. Knapen, J. E., Beckman, I. Shlosman, & T. J. Mahoney (San Francisco: ASP), 672 (astro-ph/0206398)
- Kohno, K., Ishizuki, S., Matsushita, S., Vila-Vilaro, B., & Kawabe, R., PASJ, 55, L1
- Lehnert, M. D., & Heckman, T. M. 1995, ApJS, 97, 89
- Lepp, S., & Dalgarno, A. 1996, A&A, 306, L21
- Lepp, S., & MaCray, R. 1983, ApJ, 269, 560
- Maiolino, R. et al. 2003, MNRAS, 344, L59
- Malhotra, S. et al. 1997, ApJ, 491, L27

- Malhotra, S. et al. 2000, *ApJ*, 543, 634
- Malhotra, S. et al. 2001, *ApJ*, 561, 766
- Maloney, P., Hollenbach, D., & Tielens, A. G. G. M. 1996, *ApJ*, 466, 561
- Matthews, K., & Soifer, B. T. 1994, *Infrared Astronomy with Arrays: The Next Generation*, ed. I. S. McLean (Dordrecht: Kluwer), 239
- Moorwood, A. F. M. 1986, *A&A*, 166, 4
- Mouri, H. 1994, *ApJ*, 427, 777
- Mouri, H., Kawara, K., Taniguchi, Y., & Nishida, M. 1990, *ApJ*, 356, L39
- Mouri, H., & Taniguchi, Y. 1992, *ApJ*, 386, 68
- Mouri, H., Taniguchi, Y., Kawara, K., & Nishida, M. 1989, *ApJ*, 346, L73
- Nakanishi, K., Okumura, S. K., Kohno, K., Kawabe, R., & Nakagawa, T. 2004, in *The Neutral ISM in Starburst Galaxies*, ed. S. Aalto, S. Huttemeister, A. Pedlar, in press
- Ohyama, Y., Yoshida, M., & Takata, T. 2003, *AJ*, 126, 2291
- Ohyama, Y. et al. 2000, *PASJ*, 52, 563
- Okumura, S. et al. 2000, *PASJ*, 52, 393
- Rawlings, J. M. C., Redman, M. P., Keto, E., & Williams, D. A. 2004, *MNRAS*, 351, 1054
- Rawlings, J. M. C., Taylor, S. D., & Williams, D. A. 2000, *MNRAS*, 313, 461
- Rayner, J. T., Toomey, D. W., Onaka, P. M., Denault, A. J., Stahlberger, W. E., Vacca, W. D., Cushing, M. C., & Wang, S. 2003, *PASP*, 115, 362
- Ridgway, S. E., Wynn-Williams, C. G., & Becklin, E. E. 1994, *ApJ*, 428, 609
- Rieke, G. H., Cutri, R. M., Black, J. H., Kailey, W. F., McAlary, C. W., Lebofsky, M. J., & Elston, R. 1985, *ApJ*, 290, 116
- Rieke, G. H., & Lebofsky, M. J. 1985, *ApJ*, 288, 618
- Risaliti, G., Gilli, R., Maiolino, R., & Salvati, M. 2000, *A&A*, 357, 13
- Risaliti, G., Maiolino, R., & Salvati, M. 1999, *ApJ*, 522, 157

- Robson, I. 1996, *Active Galactic Nuclei* (New York: Wiley)
- Roche P. F., & Aitken D. K. 1984, *MNRAS*, 208, 481
- Roche P. F., & Aitken D. K. 1985, *MNRAS*, 215, 425
- Roche, P. F., Aitken, D. K., Smith, C. H., & James, S. D. 1986, *MNRAS*, 218, 19p
- Roche, P. F., Aitken, D. K., Smith, C. H., & Ward, M. J. 1991, *MNRAS*, 248, 606
- Sanders, D. B., & Mirabel, I. F. 1996, *ARA&A*, 34, 749
- Sanders, D. B., Scoville, N. Z., & Soifer, B. T. 1991, *ApJ*, 370, 158
- Scoville, N. Z. et al. 2000, *AJ*, 119, 991
- Soifer, B. T., Sanders, D. B., Madore, B. F., Neugebauer, G., Danielson, G. E., Elias, J. H., Lonsdale, C. J., & Rice, W. L. 1987, *ApJ*, 320, 238
- Soifer, B. T. et al. 2000, *AJ*, 119, 509
- Spoon, H. W. W., Keane, J. V., Tielens, A. G. G. M., Lutz, D., & Moorwood, A. F. M. 2001, *A&A*, 365, L353
- Sugai, H., Malkan, M. A., Ward, M. J., Davies, R. I., & McLean, I. S. 1997, *ApJ*, 481, 186
- Takeuchi, T. T., Yoshikawa, K., & Ishii, T. T. 2003, *ApJ*, 587, L89
- Tokunaga, A. T. 2000, in *Allen's Astrophysical Quantities*, ed. A. N. Cox (4th ed; Berlin: Springer), 143
- Tokunaga, A. T., Sellgren, K., Smith, R. G., Nagata, T., Sakata, A., & Nakada, Y. 1991, *ApJ*, 380, 452
- Tsutsumi, T. Morita, K. -I. & Umeyama, S. 1997, in *Astronomical Data Analysis Software and Systems VI*, ed. G. Hunt, & H. E. Payne (San Francisco: ASP), 50
- Van der Werf, P. P., Genzel, R., Krabbe, A., Blietz, M., Lutz, D., Drapatz, S., Ward, M. J., & Forbes, D. A. 1993, *ApJ*, 405, 522
- Veilleux, S., Kim, D. -C., & Sanders, D. B. 1999a, *ApJ*, 522, 113
- Veilleux, S., Sanders, D. B., & Kim, D. -C. 1999b, *ApJ*, 522, 139
- Vignati, P. et al. 1999, *A&A*, 349, L57

Willner, S. P., Ward, M., Longmore, A., Lawrence, A., Fabbiano, G., & Elvis, M. 1984,  
PASP, 96, 143

Yao, L., Seaquist, E. R., Kuno, N., & Dunne, L. 2003, ApJ, 588, 771

Table 1. Detailed information on NGC 4418

Object	Redshift	$f_{12}$ (Jy)	$f_{25}$ (Jy)	$f_{60}$ (Jy)	$f_{100}$ (Jy)	$\log L_{\text{IR}}$ (ergs s <sup>-1</sup> )
(1)	(2)	(3)	(4)	(5)	(6)	(7)
NGC 4418	0.007	0.9	9.3	40.7	32.8	44.5

Note. — Column (1): Object. Column (2): Redshift. Columns (3)–(6):  $f_{12}$ ,  $f_{25}$ ,  $f_{60}$ , and  $f_{100}$  are *IRAS FSC* fluxes at  $12\mu\text{m}$ ,  $25\mu\text{m}$ ,  $60\mu\text{m}$ , and  $100\mu\text{m}$ , respectively. Column (7): Logarithm of infrared ( $8\text{--}1000\mu\text{m}$ ) luminosity in ergs s<sup>-1</sup> calculated with  $L_{\text{IR}} = 2.1 \times 10^{39} \times D(\text{Mpc})^2 \times (13.48 \times f_{12} + 5.16 \times f_{25} + 2.58 \times f_{60} + f_{100})$  ergs s<sup>-1</sup> (Sanders & Mirabel 1996).

Table 2. Emission lines in the  $K$ -band

Line	$\lambda_{\text{rest}}$ ( $\mu\text{m}$ )	Flux <sup>a</sup> ( $\times 10^{-15}$ ergs s $^{-1}$ cm $^{-2}$ )	Luminosity ( $\times 10^{38}$ ergs s $^{-1}$ )	FWHM (km s $^{-1}$ )	Rest EW ( $\text{\AA}$ )
(1)	(2)	(3)	(4)	(5)	(6)
H <sub>2</sub> 1–0 S(2)	2.034	3.4	3.2	220	8
H <sub>2</sub> 1–0 S(1)	2.122	13.2	13	350	36
H <sub>2</sub> 1–0 S(0)	2.223	3.9	3.7	260	12
H <sub>2</sub> 1–0 Q(1)	2.407	11.4	11	250	47
H <sub>2</sub> 1–0 Q(3)	2.424	9.5	9.0	300	39
H <sub>2</sub> 2–1 S(3)	2.074	<3.8	<3.6	500 <sup>b</sup>	<11
H <sub>2</sub> 2–1 S(1)	2.248	<3.2	<3.0	500 <sup>b</sup>	<10
Br $\gamma$	2.166	<1.7	<1.6	500 <sup>b</sup>	<6

Note. — Column (1): Line. Column (2): Rest-frame wavelength. Column (3): Observed flux. Column (4): Observed luminosity. Column (5): Full width at half maximum. Column (6): Rest-frame equivalent width.

<sup>a</sup>The flux is estimated from a Gaussian fit. We also estimate the flux by simply summing signals above an adopted continuum level, which gives values consistent within  $\sim 20\%$  for all the detected lines.

<sup>b</sup>The line width is conservatively assumed to be 500 km s $^{-1}$  to estimate the upper limit of the flux, luminosity, and rest-frame equivalent width of an emission line.

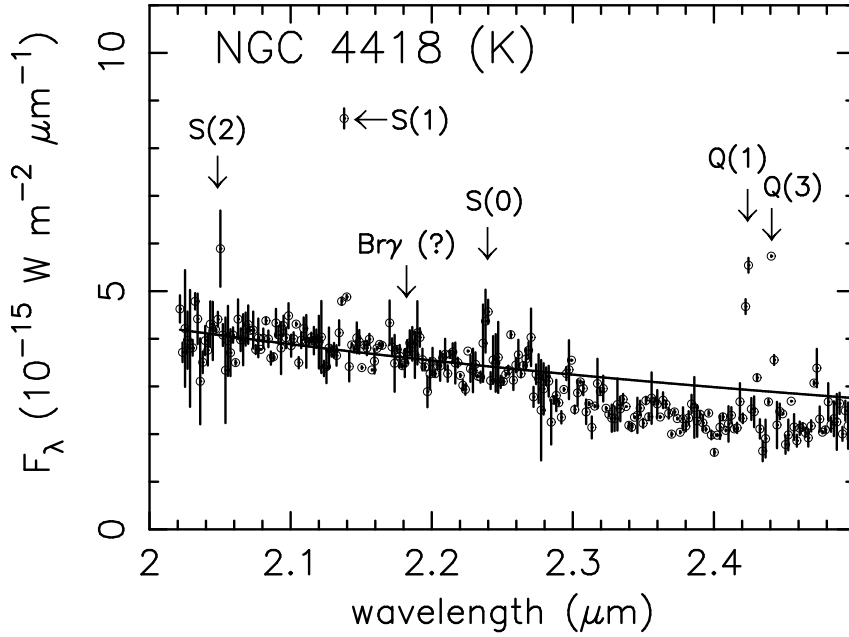


Fig. 1.— Near-infrared  $K$ -band slit spectrum of the NGC 4418 nucleus, taken with IRTF SpeX. The abscissa and ordinate are the observed wavelength in  $\mu\text{m}$  and flux  $F_\lambda$  in  $10^{-15} \text{ W m}^{-2} \mu\text{m}^{-1}$ , respectively. The solid line is the adopted continuum level with respect to which the strength of the CO absorption features is measured. Some detected  $\text{H}_2$  emission lines are indicated. S(2):  $\text{H}_2$  1–0 S(2) at  $\lambda_{\text{rest}} = 2.034 \mu\text{m}$ . S(1):  $\text{H}_2$  1–0 S(1) at  $\lambda_{\text{rest}} = 2.122 \mu\text{m}$ . S(0):  $\text{H}_2$  1–0 S(0) at  $\lambda_{\text{rest}} = 2.223 \mu\text{m}$ . Q(1):  $\text{H}_2$  1–0 Q(1) at  $\lambda_{\text{rest}} = 2.407 \mu\text{m}$ . Q(3):  $\text{H}_2$  1–0 Q(3) at  $\lambda_{\text{rest}} = 2.424 \mu\text{m}$ . The  $\text{Br}\gamma$  emission line at  $\lambda_{\text{rest}} = 2.166 \mu\text{m}$  is not clearly detected. Its expected wavelength is marked with “ $\text{Br}\gamma$  (?)”.



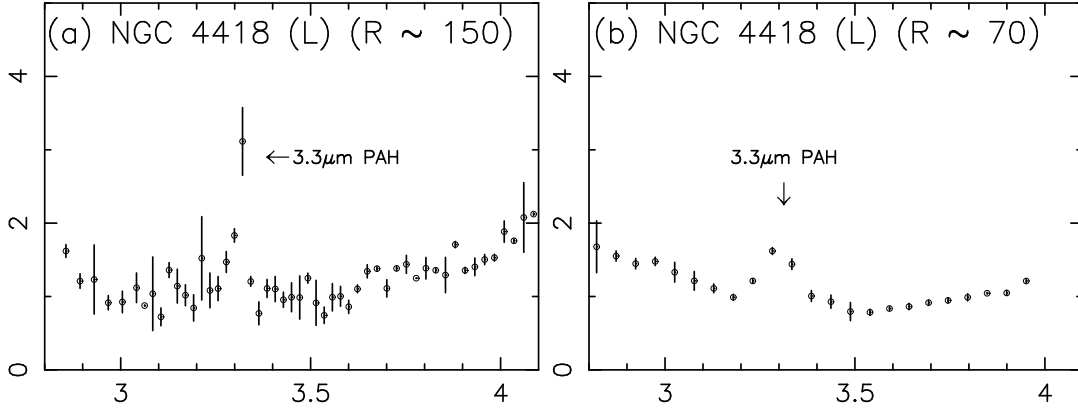


Fig. 2.— Near-infrared  $L$ -band slit spectrum of the NGC 4418 nucleus. The abscissa and ordinate are the observed wavelength in  $\mu\text{m}$  and flux  $F_\lambda$  in  $10^{-15} \text{ W m}^{-2} \mu\text{m}^{-1}$ , respectively. (a): Taken with IRTF SpeX with an aperture of  $0''.8 \times 2''.4$ . The spectral resolution is binned to  $R \sim 150$  at  $\lambda = 3.3 \mu\text{m}$ . The large error bar at the peak position of the  $3.3 \mu\text{m}$  PAH emission is likely to be caused by methane absorption at  $3.315 \mu\text{m}$  by the Earth’s atmosphere (see §2.1.2). (b): Taken with Keck I NIRC with an aperture of  $0''.7 \times 4''$ . The spectral resolution is  $R \sim 70$ .

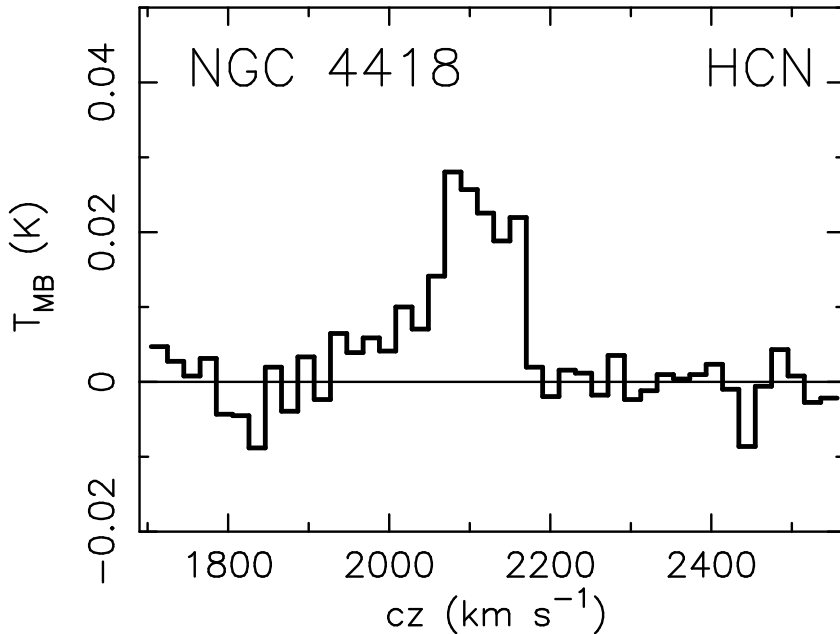


Fig. 3.— HCN (1–0) emission from NGC 4418 observed with the S100 receiver of the NRO 45m telescope (19 arcsec half-power beam width). The abscissa is velocity in  $\text{km s}^{-1}$ , and the ordinate is main beam temperature in K. The spectrum is smoothed to a velocity resolution of  $20 \text{ km s}^{-1}$ .

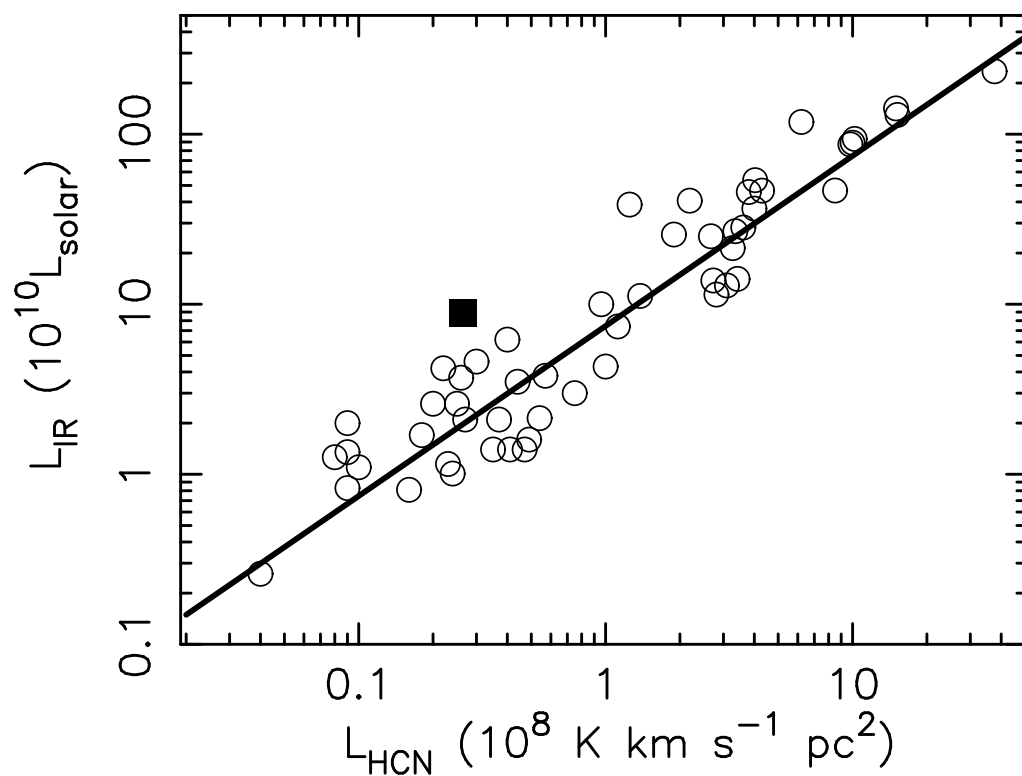


Fig. 4.— Relation between HCN (1–0) and infrared luminosity. The abscissa is HCN luminosity in  $10^8 \text{ K km s}^{-1} \text{ pc}^{-2}$  and the ordinate is infrared luminosity in  $10^{10} L_{\odot}$ . Open circles are from Gao & Solomon (2004a), and the filled square is our data of NGC 4418. The solid line is our adopted best fit line to the data by Gao & Solomon, assuming that infrared luminosity is proportional to HCN luminosity ( $L_{\text{IR}} = 7.46 \times L_{\text{HCN}}$  in the adopted units).

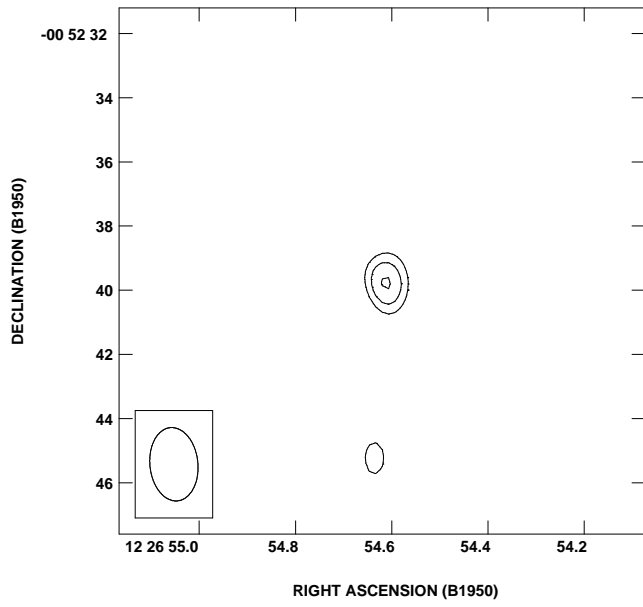


Fig. 5.— Contour map of continuum emission from NGC 4418 at  $\lambda \sim 3.4$  mm ( $\nu \sim 88$  GHz). The beam size is  $2''.3 \times 1''.5$  (position angle is  $5.8^\circ$  east of the north). Contours start at  $5.6$  mJy beam $^{-1}$  and increase in steps of  $1.4$  mJy beam $^{-1}$ .

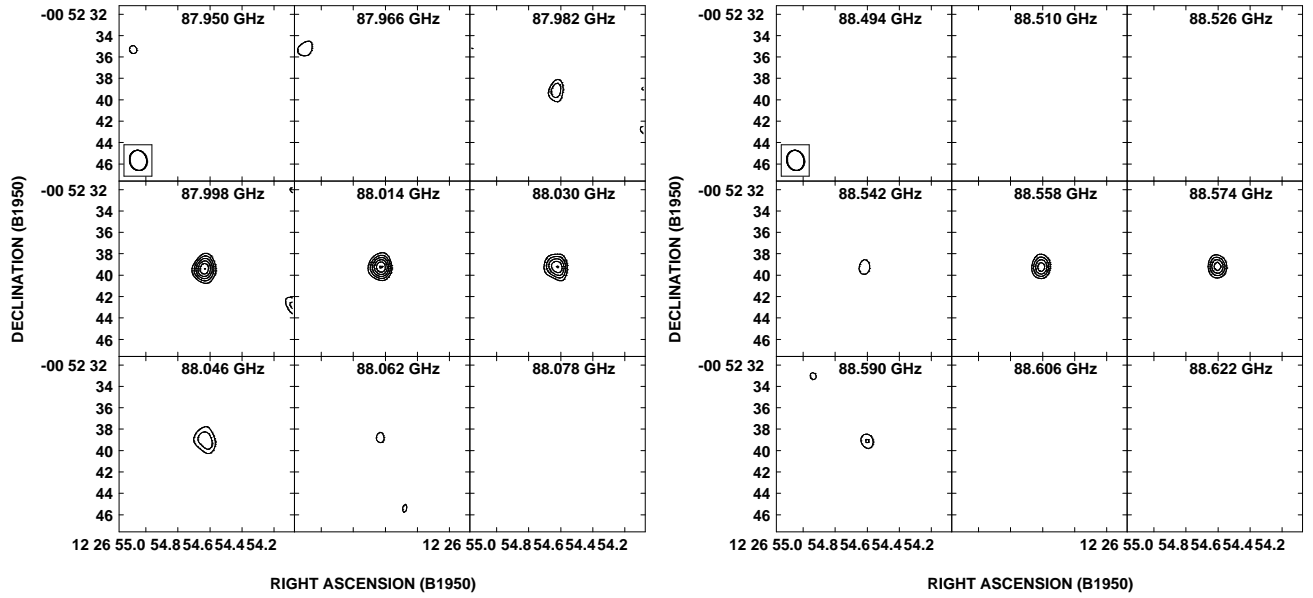


Fig. 6.— Channel maps of HCN (1–0) (*Left*) and HCO+ (1–0) (*Right*) emission lines obtained with the RAINBOW and NMA. The beam size at these lines is  $1''.9 \times 1''.6$  (position angle is  $14.7^\circ$  east of the north). Contours start at  $15 \text{ mJy beam}^{-1}$  and increase in steps of  $5 \text{ mJy beam}^{-1}$ .

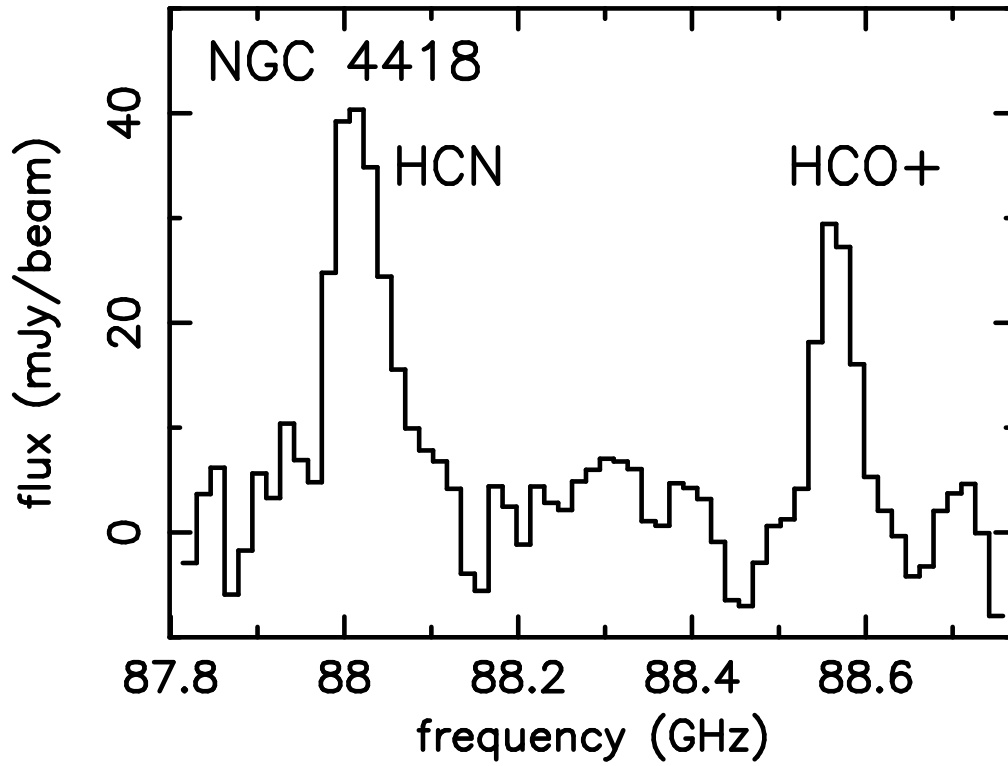


Fig. 7.— Nuclear spectrum of NGC 4418 around the HCN (1–0) and HCO+ (1–0) lines, simultaneously obtained with the RAINBOW and NMA. The spectrum is continuum-subtracted, and the CLEAN procedure was applied. The abscissa is observed frequency in GHz, and the ordinate is flux in mJy beam<sup>-1</sup>.

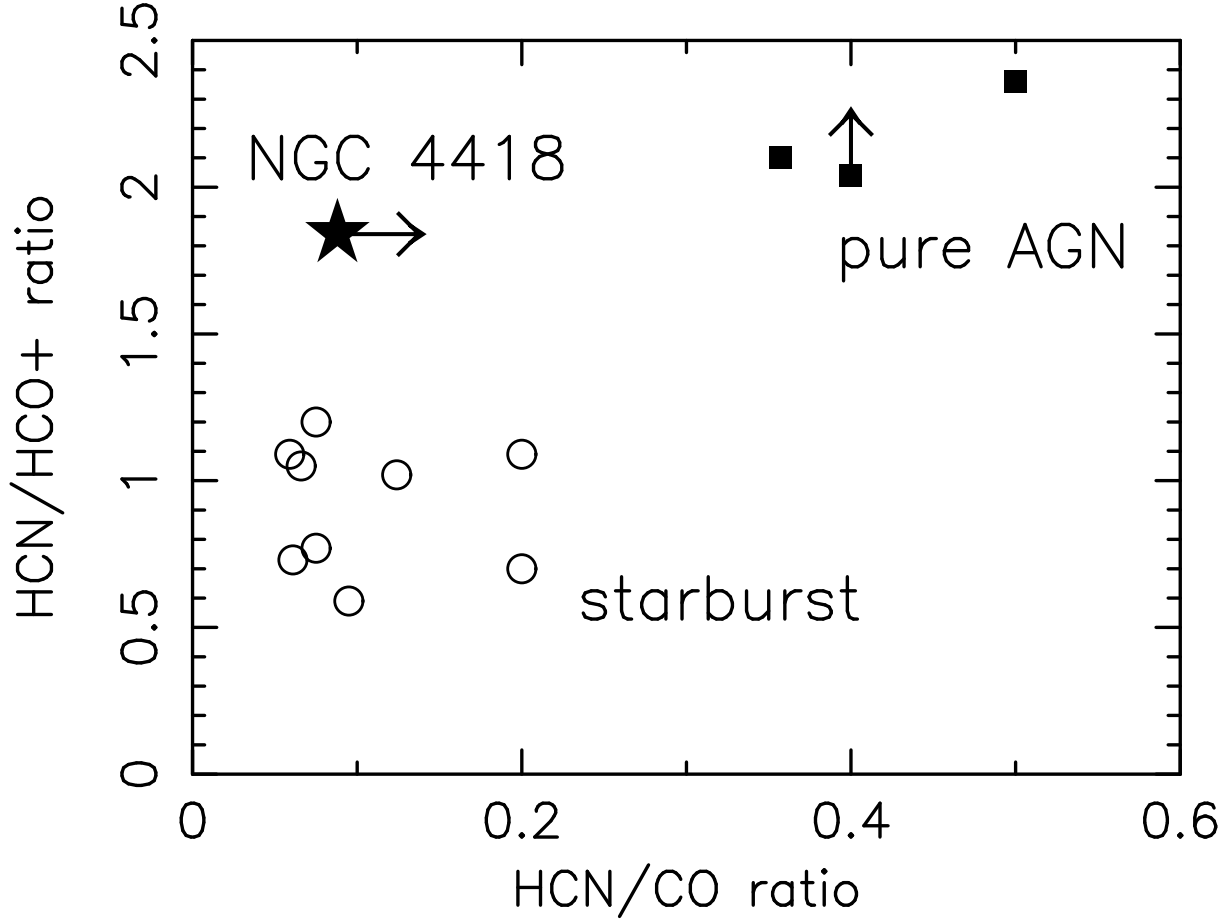


Fig. 8.— Plot of HCN (1–0) to CO (1–0) ( $\lambda_{\text{rest}} = 2.6$  mm) (abscissa) and HCN (1–0) to HCO+ (1–0) (ordinate) luminosity ratios. The data other than NGC 4418 are taken from Kohno et al. (2002). For NGC 4418, the HCN/HCO+ luminosity ratio is that directly measured toward the nucleus from our millimeter interferometric data. For the HCN/CO ratio, we adopt the values based on single dish telescopes’ measurements of CO (Sanders, Scoville, & Soifer 1991; Yao et al. 2003) and HCN (our NRO 45m data), because no interferometric observations at the CO line have been reported for NGC 4418. The single dish data reflect the global HCN/CO luminosity ratio from a significant fraction of a host galaxy. Since the molecular gas density is likely to be higher with proximity to the nucleus, it is expected that the HCN/CO ratio at the nucleus should be higher than the adopted ratio. Thus, the plotted HCN/CO should be taken as a lower limit for the actual value at the core of NGC 4418.

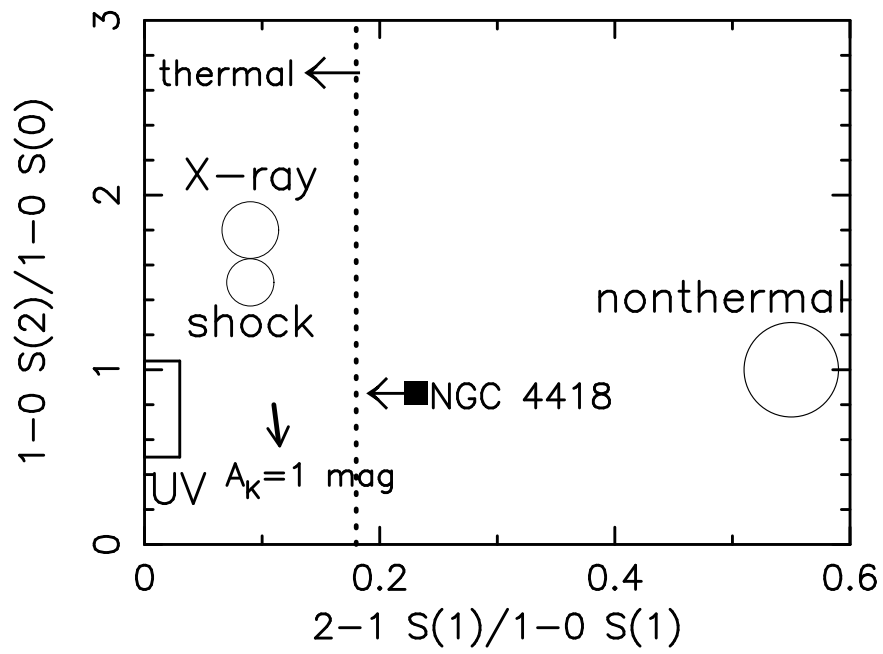


Fig. 9.— Luminosity ratios of  $H_2$  emission lines in NGC 4418. The abscissa is the 2–1 S(1) to 1–0 S(1) luminosity ratio, and the ordinate is the 1–0 S(2) to 1–0 S(0) luminosity ratio. The typical ratios for non-thermal, shock, UV, and X-ray models are indicated (Mouri 1994).